Materials Physics and Mechanics. 2023;51(3): 88-104
Research article
http://dx.doi.org/10.18149/MPM.5132023_11

Submitted: September 20, 2022
Approved: October 4, 2022
Accepted: May 7, 2023

Applied theory of bending of a functional-gradient bimorph

A.N. Soloviev [1,2], V.A. Chebanenko [2,3] ✉

[1] Don State Technical University, Rostov-on-Don, Russian Federation

[2] Southern Federal University, Rostov-on-Don, Russian Federation

[3] Federal Research Center the Southern Scientific Center of the Russian Academy of Sciences, Rostov-on-Don, Russian Federation

✉ valera.chebanenko@yandex.ru

Abstract. This paper presents a study of the stress-strain state and distribution of the electric field of a functionally gradient bimorph piezoelectric plate during its cylindrical bending. It is assumed that the layers are made of porous ceramics, the volume fraction of porosity of which varies so that its effective properties have a quadratic dependence over the plate thickness. Based on the Hamilton principle, extended to the theory of electroelasticity, a system of differential equations and boundary conditions was obtained, in which the distribution of the electric potential over the thickness of the layers is considered quadratic, and it is taken as the unknown variable in the middle of the piezoactive layer. The results of a numerical experiment based on the obtained system of equations were compared with the data of finite element modeling.

Keywords: electroelasticity, plate, bending vibrations, functionally graded piezoelectric material, porous ceramics, electric potential

Acknowledgements. *The study was supported by the grant of the Russian Science Foundation No. 22-11-00265, https://rscf.ru/project/22-11-00265/ at the Southern Federal University*

Citation: Soloviev AN, Chebanenko VA. Applied theory of bending of a functional-gradient bimorph. *Materials Physics and Mechanics*. 2023;51(3): 88-104. DOI: 10.18149/MPM.5132023_11.

Introduction

The use of piezoelectric materials from the discovery of the piezoelectric effect in 1880 to the present day has become widespread in various fields of science, industry, aerospace, medicine, acoustics, MEMS, etc. Such interest in piezoactive materials is due to the fact that they quite effectively convert both electrical energy into mechanical energy and vice versa. The main advantages that have provided such a wide use of piezoelectric materials are good electromechanical properties, durability, relative ease of manufacture, as well as flexibility in the process of designing and integrating devices based on them. In this regard, the main areas of application are monitoring the state of structures, the emission and reception of acoustic waves, active suppression of parasitic vibrations, piezoelectric motors and actuators, various sensors for measuring mechanical quantities, as well as energy harvesting. Energy harvesting means the conversion of free unused energy of mechanical vibrations present in structures into electrical energy, and its subsequent accumulation. A more detailed overview of various areas of application of piezoelectric transducers is given in [1–3].

Publisher: Peter the Great St. Petersburg Polytechnic University

The most common design for bending mode piezoelectric devices has become multilayer transducers. A special case of this type of transducers is a bimorph, which consists of two layers of piezoelectric material, between which there can also be a purely elastic layer.

Layered structures have a significant drawback, which is a high concentration of mechanical stresses near the interlayer surfaces due to abrupt changes in the composition of materials. Such a concentration of stresses can lead to a serious deterioration in both the strength of the interlaminar connection and the output characteristics. To solve this problem, for the first time in 1995, a new type of actuators was developed [4], in which one or more layers were made of piezoelectric materials, whose physical properties were not uniform in thickness. Piezoactive materials whose physical properties have a non-uniform distribution in one or more directions are called functionally graded piezoelectric materials (FGPMs). Various FGPM production methods were further developed, on the basis of which more efficient actuators were made [5–8]

Research in the field of modeling layered piezoactive structures has been carried out for a relatively long time. There are various mathematical models in the literature that describe the operation of a piezoelectric sensor, an actuator, and a generator. In early works [9,10] studied the static cylindrical bending and free vibrations of piezoelectric transducers based on the analytical solutions of the equations of the theory of electroelasticity in a three-dimensional formulation. However, for an arbitrary transducer geometry, obtaining such analytical solutions can be a rather difficult problem. In some works [11,12] to simplify the problem, induced deformation was used in the process of modeling the stress-strain state of the actuator. However, this simplification does not allow modeling the distribution of the electric field, since the electric potential is not considered as a variable, which does not allow obtaining a fully coupled electromechanical response. Another approach that allows modeling piezoelectric devices with arbitrary geometry is the finite element (FE) method [13–17]. However, one of its main disadvantages is the need for large computing power in three-dimensional problems, where the thickness of one layer may be much less than other geometric dimensions of the structure.

In problems associated with modeling piezoelectric devices such as actuators [18] and piezoelectric generators [19], the hypothesis of a linear distribution of the electric field over the thickness of the piezoactive layer is often used. However, in some cases of piezoelectric elements with thickness polarization [17] and in layered piezoelectric composites [20], shear stresses can arise, which can directly affect the distribution of the electric potential. Therefore, the use of a nonlinear form of the electric potential is also necessary in a number of problems. For example, there are works [21,22] associated with the modeling of multilayer piezoelectric plates, where the distribution of the electric potential over the thickness of the plate is assumed to be nonlinear.

Modeling of vibrations of FGPM structures is given special attention in the literature. Thus, the authors of [23], in the course of studying the problem of bending a functionally graded piezoelectric (FGP) cantilever beam under various loads, determined the stress and induction functions in the form of polynomials. The piezoelectric beam they studied was characterized by smoothly varying properties in terms of one elastic parameter and material density. In [24], the static bending, free vibrations and dynamic response of monomorphic, bimorphic and multimorphic actuators made of FGPM under combined thermoelectromechanical loading based on the Timoshenko beam theory were studied. It was assumed that the distribution of material properties over the thickness is nonuniform. It was found that shear deformations should be taken into account when the beam length to thickness ratio is less than 5. Based on the Hamilton principle and Donnell's theory of nonlinear shells, the authors of [25] studied the nonlinear multiple resonances of FGP shells containing microvoids. Their results show that external applied stress, temperature change, external

excitation and porosity volume fraction play a significant role in the non-linear vibration response. In [26], based on the method of energy decomposition of domains, the dynamic behavior of a stepped FGP plate with arbitrary boundary conditions was studied in the framework of first-order shear deformation theory. The main idea of the method was that rectangular plates were segmented in the length direction using segmentation technology, so as to obtain a stepped FGP plate, provided that the thickness of each sub-domain was specified differently. In [27], the authors, based on the principle of virtual work, obtained the basic equations and boundary conditions that describe the bending of an FGP plate using a simple quasi-three-dimensional theory of shear deformation. Parametric studies were carried out to investigate the effect of plate thickness and electric field on the overall electromechanical response of FGP plates. Using the finite element method (FEM) with a scalable boundary, in [28], for the first time, analytical solutions are presented for the transverse free vibrations of FGP composite plates. FGPM inhomogeneity distributions are presented as arbitrary mathematical expressions with respect to one or two directions in the plane.

There are works devoted to the study of functionally graded piezoactive porous plates. In [29], where vibrations of porous FGP plates were studied, a modified power law was used to describe the properties of the material. The authors of [30] presented the isogeometric FE Bezier method in combination with the theory of high-order shear for vibration analysis of FGPM plates. The material properties of the FGP plates change continuously in the thickness direction and are calculated using a modified power law. The paper [31] investigated the characteristics of free vibrations of a bidirectional FGP porous plate subjected to thermal and electrical loading using the FEM. The properties of the plate varied as power-law distributions in two directions, that is, in the longitudinal and transverse directions. In the works cited, a significant influence of the distribution of porosity on the integral and field characteristics of piezoelectric transducers is noted.

The researchers are also considering applications for FGP converters in the energy harvesting field. For example, work [32] is devoted to energy harvesting using an FGP beam. It is assumed that the material properties of the FGP plate vary in thickness according to a power law. It has been found that there is a value of the exponent index at which the maximum output power is achieved. In addition, there is a power index value, after which a further increase in the power index value has little effect on the output power. The aim of [33] was to study the frequency of static bending and vibration FGP of a nanobeam with a dynamic flexoelectric effect. Numerical results show that the dynamic flexoelectric effect is significant in the study of higher-order vibration modes of the FGP nanobeam, while the exponent index has a significant effect on the dimensionless frequency of each mode. It should be noted the work [34], which presents a practical approach to the fabrication of an FGP storage device, as well as a new concept of energy harvesting from composite piezoelectric materials using materials with a gradient structure, which have a high energy harvesting efficiency.

From the review above, we can conclude that the use of a nonlinear form of the electric potential, which takes into account its inhomogeneity, both in thickness and in the longitudinal direction, may be necessary in the problems of modeling vibrations of FGP plates and multilayer transducers. Since the heterogeneity of the distribution of physical properties in FGP materials can directly affect the nature of the distribution of mechanical and electrical fields of such transducers.

Previously, we developed an applied theory of vibrations of piezoelectric bimorphs [35], which used a quadratic distribution of the electric potential over the thickness, and also took into account the nonlinearity of the distribution in the longitudinal direction. Comparison of the results based on the developed theory with the data of the FE analysis in

the problems of calculating steady-state oscillations and resonant frequencies showed good agreement.

In [36], for an analytical model of an energy harvesting device in the FE package ACELAN-COMPOS, the effective properties of porous piezoceramics were calculated. In this paper, we will present an applied theory describing the vibrations of a cantilever FGP bimorph, in which the volume fraction of porosity varies so that the effective properties of ceramics have a quadratic dependence over the plate thickness. The study will show the effect of various types of loading and volume fraction of porosity on the electric potential and stress-strain state, as well as on natural frequencies. To test the results of the applied theory, a comparison will be made with a similar problem built in the COMSOL Multiphysics package.

Problem statement

We will consider a plane problem of steady bending vibrations of a bimorph piezoelectric plate, the layers of which are polarized along the thickness (x_3 axis). We set the origin of coordinates at the left edge of the plate (Fig. 1).

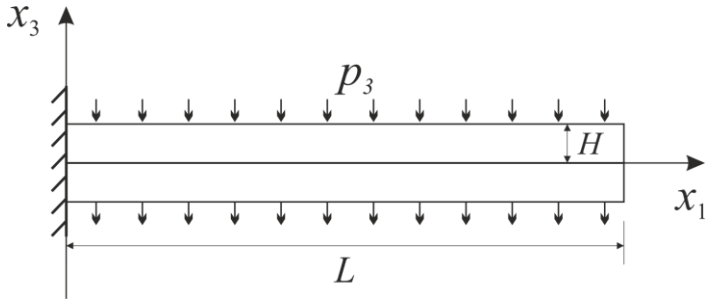

Fig. 1. Diagram of the cantilever

It is assumed that electrodes are deposited on the outer $x_3 = \pm H$ and inner $x_3 = 0$ boundaries of the layers, parallel to the x_1 axis (Fig. 1). We assume that the electrodes are connected in parallel: external to external, internal to internal. Excitation in the system occurs due to a distributed mechanical load p_3 with a circular frequency ω.

Oscillations of an electroelastic medium are described by the following system of differential equations [37]:

$$\begin{aligned} &\sigma_{ij,j} + \rho\omega^2 u_i = F_i, \\ &D_{i,i} = 0, \end{aligned} \tag{1}$$

where σ_{ij} are the stress tensor components; ρ is the density of the material, u_i are components of the displacement vector, D_i are components of the vector of electric induction and F_i is vector of body forces.

We consider that the right side surface of the plate is free from stresses $\sigma_{11} = \sigma_{13} = 0$, and the left side is rigidly clamped. It is assumed that there are no charges on non-electrodated surfaces, so $D_1 = 0$ at $x_1 = 0$ and $x_1 = L$.

Since we are considering a two-dimensional problem, the constitutive relations for a piezoelectric medium are noticeably simplified:

$$\begin{aligned}
&\sigma_{11} = c_{11}^{E}\varepsilon_{11} + c_{13}^{E}\varepsilon_{33} + e_{31}\varphi_{,3},\\
&\sigma_{33} = c_{13}^{E}\varepsilon_{11} + c_{33}^{E}\varepsilon_{33} + e_{33}\varphi_{,3},\\
&\sigma_{13} = 2c_{44}^{E}\varepsilon_{13} + e_{31}\varphi_{,1},\\
&D_1 = 2e_{15}\varepsilon_{13} - \epsilon_{11}^{S}\varphi_{,1},\\
&D_3 = e_{31}\varepsilon_{11} + e_{33}\varepsilon_{33} - \epsilon_{33}^{S}\varphi_{,3},
\end{aligned} \tag{2}$$

where c_{ij}^{E} are elastic moduli measured at constant electric field, ε_{ij} are strain tensor components, e_{ij} are piezoelectric constants, φ is electric potential, ϵ_{ij}^{S} are permittivities measured at constant strain.

Next, a FGPM is considered, for example, associated with inhomogeneous porosity in thickness. Therefore, the dependence of the material properties described above on the x_3 coordinate is assumed.

For further reasoning, it is necessary to accept the Kirchhoff hypotheses, according to which the components of the displacement vector take the following form

$$\begin{aligned}
&u_1(x_1, x_3) = -x_3 w_{,1},\\
&u_3(x_1, x_3) = w(x_1),
\end{aligned} \tag{3}$$

where $w(x_1)$ is the deflection function of the middle surface of the plate.

According to the accepted hypotheses, it is assumed that the normal stress σ_{33} is equal to zero everywhere in the area of the plate. Accordingly, there is an opportunity for further simplification by excluding the deformation tensor component ε_{33} from the constitutive relations (1):

$$\begin{aligned}
&\sigma_{11} = c_{11}^{*}u_{1,1} + e_{31}^{*}\varphi_{,3},\\
&D_3 = e_{31}^{*}u_{1,1} - \epsilon_{33}^{*}\varphi_{,3},
\end{aligned} \tag{4}$$

here

$$\begin{aligned}
&c_{11}^{*} = c_{11}^{E} - \frac{c_{13}^{E\,2}}{c_{33}^{E}},\\
&e_{31}^{*} = e_{31} - \frac{c_{13}^{E} e_{33}}{c_{33}^{E}},\\
&\epsilon_{33}^{*} = \epsilon_{33}^{S} + \frac{e_{33}^{2}}{c_{33}^{E}}.
\end{aligned} \tag{5}$$

The expressions for σ_{13} and D_1 will remain unchanged. As the law of distribution of material properties over the thickness, we will consider quadratic. To take into account the quadratic distribution over the layer thickness, we introduce the shape function for the material constants of the following form

$$Y(a, \hat{a}, x_3) = \frac{(\hat{a} - a)}{H^2} x_3^2 + a, \tag{6}$$

where a corresponds to the value of the material constant at the center of the plate and $\hat{a}$ corresponds to the constant near the surface. Here and below, a cap over the designations of material constants will mean that the constant corresponds to the outer boundary, and the absence of a cap, to the inner boundary. As an example, Fig. 2 shows the distribution of the elastic modulus c_{11} over the bimorph thickness, where $\hat{c}_{11}$ = 2.93 GPa and c_{11} = 9.1 GPa.

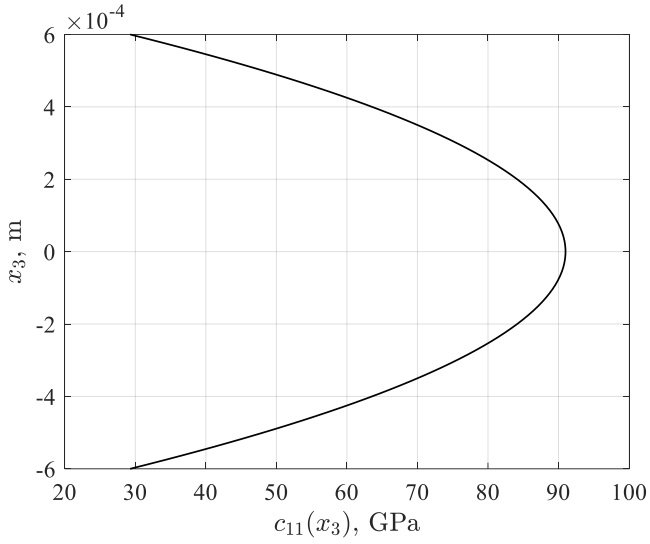

Fig. 2. Distribution c_{11} over plate thickness

Then the constitutive relations and the density change as follows

$$\begin{aligned}
&\sigma_{11} = Y(c_{11}^{*}, \hat{c}_{11}^{*}, x_3)u_{1,1} + Y(e_{31}^{*}, \hat{e}_{31}^{*}, x_3)\varphi_{,3},\\
&D_3 = Y(e_{31}^{*}, \hat{e}_{31}^{*}, x_3)u_{1,1} - Y(\epsilon_{33}^{*}, \hat{\epsilon}_{33}^{*}, x_3)\varphi_{,3},\\
&D_1 = -Y(\epsilon_{11}^{S}, \hat{\epsilon}_{11}^{S}, x_3)\varphi_{,1},\\
&\rho = Y(\rho, \hat{\rho}, x_3).
\end{aligned} \tag{7}$$

It should be noted that in the case when the constants at the surface and in the center of the plate are equal, then the distribution of properties of the material becomes constant.

In the previous work [35], it was shown that the use of the quadratic form of the potential distribution makes it possible to model the electric field more accurately in problems of bending vibrations of a bimorph. Accounting for the electrical boundary conditions at $x_3 = \pm H$, $x_3 = 0$ and the value of the potential in the middle of the layers $x_3 = \pm H/2$ are also implemented in our proposed quadratic form of the electrical potential:

$$\varphi(x_1, \tilde{x}_3) = V_1(x_1)\frac{\tilde{x}_3}{H}\left(\frac{2\tilde{x}_3}{H} - 1\right) + V_2(x_1)\left(1 - \frac{4\tilde{x}_3^2}{H^2}\right) + V_3(x_1)\frac{\tilde{x}_3}{H}\left(\frac{2\tilde{x}_3}{H} + 1\right). \tag{8}$$

Here $\tilde{x}_3 = x_3 - H/2$. For the lower layer, the distribution will be similar, but $\tilde{x}_3 = x_3 + H/2$.

Within the framework of the problem under study, we will assume the following case. The potential is either given at the electrodes or is an unknown constant, while in the middle of the layer it is an unknown function:

$$\begin{aligned}
&\varphi(x_1, 0) = V_1 = const,\\
&\varphi\left(x_1, \frac{H}{2}\right) = V_2(x_1) = \Phi(x_1),\\
&\varphi(x_1, H) = V_3 = const.
\end{aligned} \tag{9}$$

Here $\Phi(x_1)$ is the unknown potential distribution function in the middle of the layer in the direction of the x_1 axis.

For further construction of an applied theory, we use the Hamilton principle for an electroelastic medium. In the case of plane deformation in the presence of surface loads and the absence of surface charges, the variational equation takes the form [37]:

$$\iint\limits_S \delta \breve{H} dS - \rho\omega^2 \iint\limits_S u_i \delta u_i dS + \int\limits_{\partial S} p_i \delta u_i dl = 0, \tag{10}$$

where $\breve{H} = U - E_i D_i$ is the electric enthalpy whose variation is equal to $\delta\breve{H} = \sigma_{ij}\delta\varepsilon_{ij} - D_i\delta E_i$, S is the bimorph region, ∂S is the boundary of the bimorph region.

Taking into account the accepted hypotheses (3), the enthalpy variation takes the following form:

$$\delta\breve{H} = \sigma_{11}\delta\varepsilon_{11} - D_1\delta E_1 - D_3\delta E_3. \tag{11}$$

The distributed load that creates excitation in the system under consideration is given by the vector $p_i = \left(0, p_3\right)^T$. After varying the equation (11), we substitute it into (10). Integration over the thickness eliminates the dependence on x_3, so in what follows we omit the subscript of x_1. At the next step, in the integrands, we equate the coefficients at δw and $\delta\Phi$. From here we get a system of differential equations with constant coefficients:

$$\begin{aligned}
&\left(\frac{4}{5H}\epsilon_{33}^* + \frac{68}{15H}\hat{\epsilon}_{33}^*\right)V_1 + \left(\frac{52}{15H}\epsilon_{33}^* + \frac{28}{15H}\hat{\epsilon}_{33}^*\right)V_3 - \left(\frac{32}{5H}\hat{\epsilon}_{33}^* + \frac{64}{15H}\epsilon_{33}^*\right)\Phi(x) - \\
&\quad - \left(\frac{16}{21}\hat{\epsilon}_{11}H + \frac{32}{105}\epsilon_{11}H\right)\frac{d^2}{dx^2}\Phi(x) - \left(\frac{2}{15}\hat{e}_{31}^*H + \frac{6}{5}e_{31}^*H\right)\frac{d^2}{dx^2}w(x) = 0, \\
&\left(\frac{2}{15}\hat{e}_{31}^*H + \frac{6}{5}e_{31}^*H\right)\frac{d^2}{dx^2}\Phi(x) + \left(\frac{4}{15}\omega^2\hat{\rho}H^3 + \frac{2}{5}\omega^2\rho H^3\right)\frac{d^2}{dx^2}w(x) - \\
&\quad - \left(\frac{2}{3}\omega^2\rho H + \frac{4}{3}\omega^2\hat{\rho}H\right)w(x) + \left(\frac{4}{15}\hat{c}_{11}^*H^3 + \frac{2}{5}c_{11}^*H^3\right)\frac{d^4}{dx^4}w(x) + 2p_3 = 0.
\end{aligned} \tag{12}$$

Equating to zero the coefficients for independent variations in the non-integral terms, we obtain expressions for internal force (M_1 and Q_1) and electrical ($\tilde{D}_1$) factors used in natural boundary conditions:

$$\begin{aligned}
\tilde{D}_1 &= \left(\frac{16}{21}\hat{\epsilon}_{11}H + \frac{32}{105}\epsilon_{11}H\right)\frac{d}{dx}\Phi(x), \\
M_1 &= \left(-\frac{1}{10}e_{31}^*H + \frac{13}{30}\hat{e}_{31}^*H\right)V_1 - \left(\frac{17}{30}\hat{e}_{31}^*H + \frac{11}{10}e_{31}^*H\right)V_3 + \left(\frac{2}{15}\hat{e}_{31}^*H + \frac{6}{5}e_{31}^*H\right)\Phi(x) + \\
&\quad + \left(\frac{4}{15}\hat{c}_{11}^*H^3 + \frac{2}{5}c_{11}^*H^3\right)\frac{d^2}{dx^2}w(x), \\
Q_1 &= -\left(\frac{2}{15}\hat{e}_{31}^*H + \frac{6}{5}e_{31}^*H\right)\frac{d}{dx}\Phi(x) - \left(\frac{4}{15}\omega^2\hat{\rho}H^3 + \frac{2}{5}\omega^2\rho H^3\right)\frac{d}{dx}w(x) - \\
&\quad - \left(\frac{2}{5}c_{11}^*H^3 + \frac{4}{15}\hat{c}_{11}^*H^3\right)\frac{d^3}{dx^3}w(x).
\end{aligned} \tag{13}$$

Results and discussion

Using the obtained model, we study a plate made of porous piezoceramic PZT-4, shown in Fig. 1. It is assumed that the layers of the plate were made in such a way that the distribution of properties (5) over the thickness acquired a quadratic character.

The system of ordinary differential equations with constant coefficients (12), which describes the bending vibrations of the FGP bimorph plate, can be solved analytically or

numerically, for example, using the shooting method. To verify the theory obtained, we will compare it with the results of calculations based on the FEM implemented in the COMSOL Multiphysics package (CKP SSC-RAS № 501994). When modelling in COMSOL, a module for solving partial differential equations in a general form was used. Within the framework of the FEM, a plane problem of vibrations of an electroelastic bimorph was considered, in which all material constants in the constitutive relations (2) were described by the shape function (6). The values of material constants for different degrees of porosity within the framework of this work are given in Table 1. The constants were taken from the article [36], where they were calculated for PZT-4 ceramics from 0 to 80 % with a step of 10.

Table 1. Material constants for PZT-4 with different degrees of porosity [36]

Porosity, %	0	10	20	30	40	50	60	70	80
ρ, kg/m^3	7500	6750	6000	5250	4500	3750	3000	2250	1500
c_{11}^E, GPa	139	115.6	92.5	68.5	50.5	33.4	20.7	12.6	6.8
c_{12}^E, GPa	77.8	61.5	46.6	31.4	21	11.6	6.2	2.8	1.3
c_{13}^E, GPa	74.3	58.2	42.5	28.2	18.7	10.6	5.2	2.4	1
c_{33}^E, GPa	115	95.3	72.3	54.2	39.1	27.2	16.3	9.1	4.7
c_{44}^E, GPa	25.6	22.3	18.3	14.4	11	7.4	4.4	2.3	1
e_{31}, pC/N	-5.2	-4.23	-3.14	-2.07	-1.32	-0.75	-0.43	-0.21	-0.1
e_{33}, pC/N	15.1	13.38	11.37	9.59	7.68	5.93	3.93	2.3	1.25
e_{15}, pC/N	12.7	10.96	8.96	6.91	5	3.3	1.95	1	0.44
$\epsilon_{11}^S / \epsilon_0$	730	663	582	509	439	349	263	191	122
$\epsilon_{33}^S / \epsilon_0$	635	567	492	413	345	270	199	130	75

Within the framework of numerical calculations, cases will be investigated when the porosity changes from lower near the surface of the plate to higher inside and vice versa. To simplify the notation, we will call “case I” the situation when the porosity at the surface of the plate is 0 %, and in the center 50 %. The opposite configuration, when the porosity at the plate surface will be 50 %, and inside 0 %, we will call “case II”. Two types of vibration excitation will also be considered: mechanical and electrical.

Due to the symmetry of the plate about the x_1 axis, to simplify the problem, only one upper layer can be considered. For the main characteristics, we take the values that will refer to the upper layer, such as the distribution of the electric potential over the thickness of the layer at the central point of the plate $\varphi(L/2, x_3)$ and along the x_1 axis $\varphi(x_1, H/2) = \Phi(x_1)$, the distribution of mechanical stresses over the thickness of the layer at the central point of the plate $\sigma_{11}(L/2, x_3)$, and the deflection of the middle surface $w(x_1)$. On thickness plots, the $x_3 = 0$ coordinate will correspond to the neutral surface. In addition, the natural frequencies of the plate will also be studied.

To begin with, we study case I with mechanical excitation of the plate. Let us consider plate oscillations at a frequency of 50 Hz under a load $p = 1$ N/m, provided that $V_1 = V_3 = 0$ V.

The data presented in Fig. 3 indicate that when the ceramic porosity changes from less near the surface to more inside the plate, the applied theory accurately describes the behavior of the studied characteristics. In Figure 3(b), one can notice a small jump in the electrical potential in the clamping area, and the shape of the longitudinal distribution itself is non-

linear. In addition, in Fig. 3(d), there is a slight deviation of the electric potential distribution plot according to the applied theory from the FE simulation data, and the distribution form itself is quadratic. Next, consider the same problem for case II.

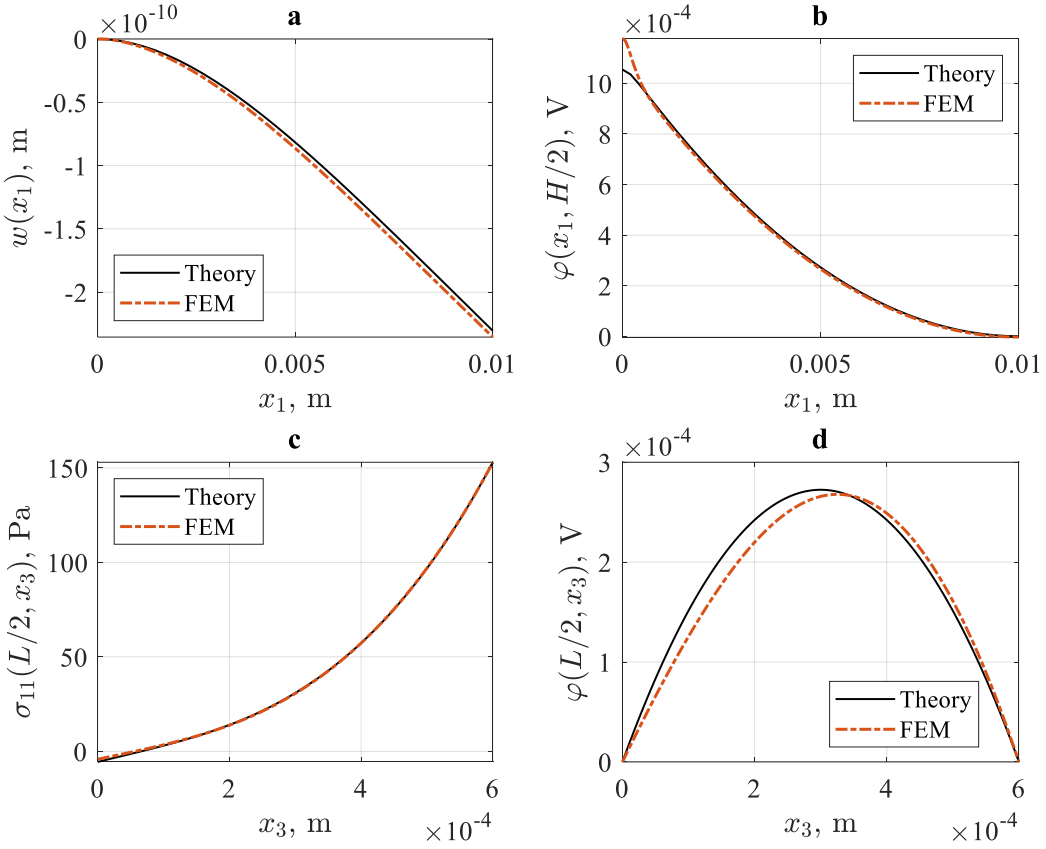

Fig. 3. Comparison of numerical results obtained on the basis of FEM and applied theory. Dependencies: a) deflection on x_1, b) electric potential on x_1 at $H/2$, c) mechanical stresses on x_3 at $L/2$, d) electric potential on x_3 at $L/2$

Based on the data in Fig. 4, it can be concluded that when the ceramic porosity changes from larger at the surface to smaller inside the plate, the applied theory describes the mechanical characteristics quite well. Figure 4(d) shows that, according to the FE simulation data, the distribution of the electric potential has a clearly non-quadratic character. From which we can conclude that in this case the quadratic distribution accepted in the theory does not describe the behavior of the electric potential well enough. Also, it can be noted that the mechanical stresses shown in Fig. 4(c) have a local maximum closer to the surface.

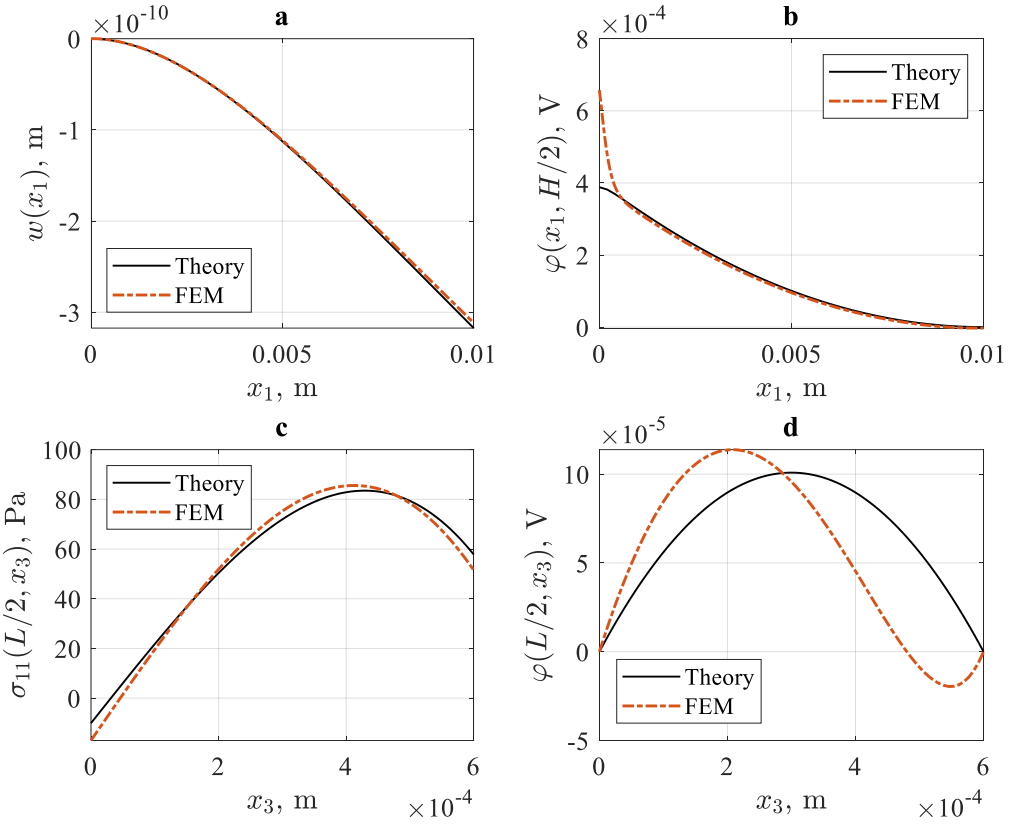

Fig. 4. Comparison of numerical results obtained on the basis of FEM and applied theory. Dependencies: a) deflection on x_1, b) electric potential on x_1 at $H/2$, c) mechanical stresses on x_3 at $L/2$, d) electric potential on x_3 at $L/2$

In a previous study [35], it was shown that in the case when a non-zero potential is present, the accuracy of the applied theory increases. Therefore, at the next stage of the numerical experiment, we will study the oscillations of the plate under the influence of the electric potential for two cases of porosity distribution.

In the framework of case I, we consider plate vibrations at a frequency of 50 Hz, under the condition $V_1 = 0$ and $V_3 = 1$ V.

The data in Fig. 5 indicate a fairly good convergence of the results. The plate deflection shown in Fig. 5(a) is calculated with a high degree of accuracy. It should be noted that in Fig. 5(b), as in all previous cases studied, the error is localized near the edges of the plate, and the main part of the electric potential distribution in the longitudinal direction is constant. The distribution of mechanical stresses over the thickness in the center of the plate, shown in Fig. 5(c), is more complex than the linear one observed for the purely elastic case in the absence of gradients in material properties. The distribution of the electric potential over the thickness, shown in Fig. 5(d), is also quadratic, but already tends to be linear.

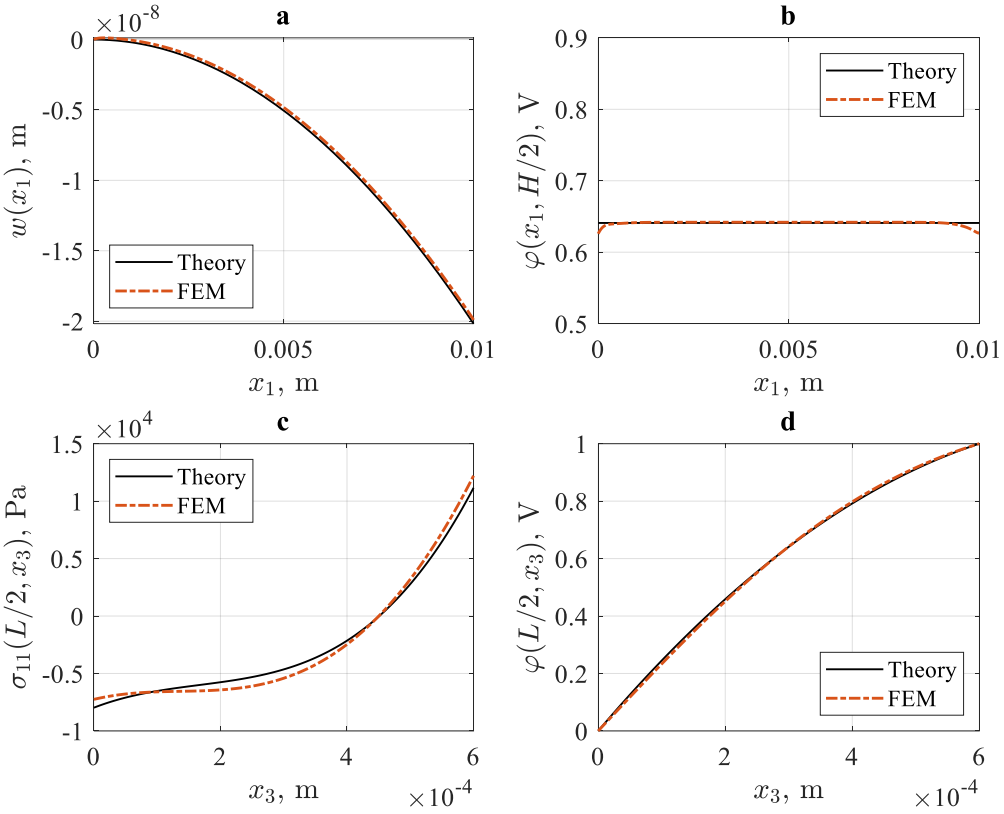

Fig. 5. Comparison of numerical results obtained on the basis of FEM and applied theory. Dependencies: a) deflection on x_1, b) electric potential on x_1 at $H/2$, c) mechanical stresses on x_3 at $L/2$, d) electric potential on x_3 at $L/2$

At the end of this stage of research, we consider case II under the same boundary conditions.

As can be seen from Fig. 6(b), the error in finding the longitudinal distribution of the electric potential has increased, and the nature of the jumps at the edges of the plate has changed compared to the previous case. However, the shape of most of the distribution remained constant. It can also be noted that the error in finding the distribution of longitudinal mechanical stresses, presented in Fig. 6(c), has slightly increased. Figure 6(d) shows that in the presence of a given potential difference across the electrodes, the shape of the electric potential distribution over the thickness tends to be linear. Previously, it was found that in case II at zero values of the electric potential, the results of the calculation according to the applied theory demonstrate a significant error in finding the electric potential. On the contrary, under the condition that one of the potentials is nonzero, for case II, the applied theory has demonstrated fairly good convergence with the FE calculation.

In conclusion, consider the case when the potential V_3 on the outer electrodes is unknown, the plate is subjected to a distributed load $p_3 = 1$ N/m with a frequency of 50 Hz, and the inner electrode is grounded $V_1 = 0$. To find the unknown potential, you need to add the condition:

$$\int_{\partial S_E} D_3 ds = 0, \tag{14}$$

where ∂S_E is the electroded boundary of the bimorph region.

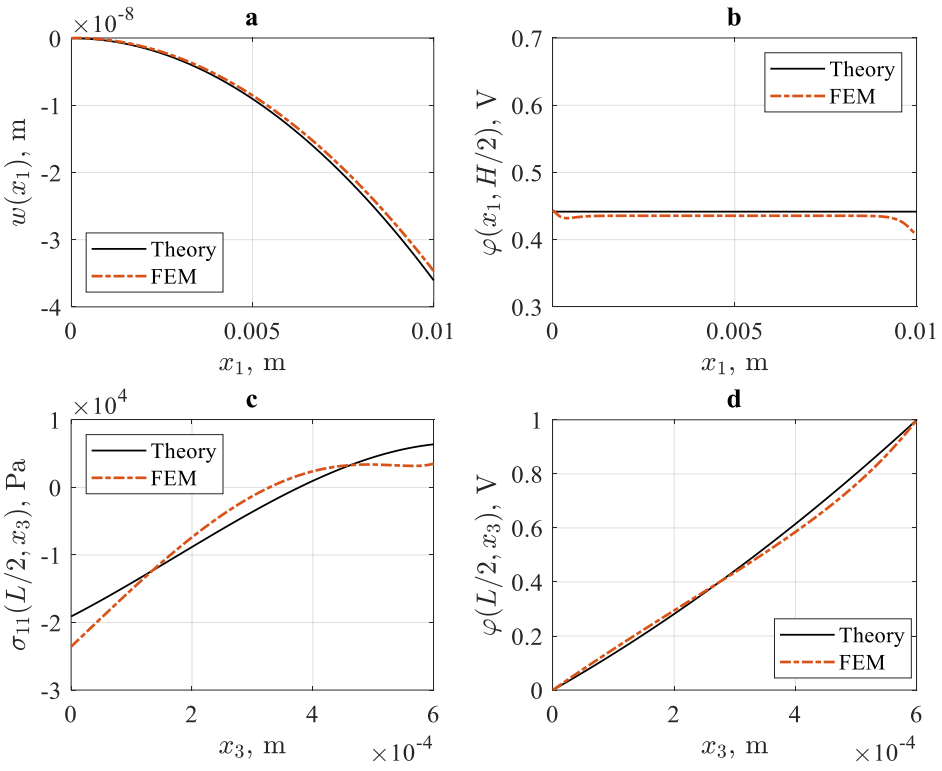

Fig. 6. Comparison of numerical results obtained on the basis of FEM and applied theory. Dependencies: a) deflection on x_1, b) electric potential on x_1 at $H/2$, c) mechanical stresses on x_3 at $L/2$, d) electric potential on x_3 at $L/2$

Figure 7 shows that in the case when the potential at the external electrodes is unknown, and the porosity of the ceramic changes from higher near the surface to lower inside the plate, the applied theory quite accurately describes the behavior of mechanical and electric fields. Figure 7(b) shows that the main error is localized at the edges of the plate, and the distribution itself is nonlinear, as in the case of mechanical loading at zero potentials on the electrodes. As in the previous case, Fig. 7(c) shows a local maximum of mechanical stresses. It should be noted that the distribution of the electric potential over the thickness, shown in Fig. 7(d), has a quadratic character, which is well described by the quadratic distribution adopted in the work. Case I was also considered, which showed good results, which will not be given here, since its results are similar to the cases already studied.

In Figures 4(b) and 7(b), jumps in the electric potential near the clamping area and at the free edge can be noted, which are not described by this theory. These jumps are due to the fact that the Kirchhoff hypotheses adopted in the work exclude shear stresses from consideration, while they are preserved in the FE model [38]. However, the areas of these discrepancies do not exceed the thickness of the plate. As noted in [24], shear stresses must be taken into account under the condition $L/H < 5$, and in our case $L/H = 8.3$.

At the last stage, we will study the natural frequencies of the plate using the proposed theory for various degrees of porosity and compare them with the data of FE calculations. The results are presented in Table 2.

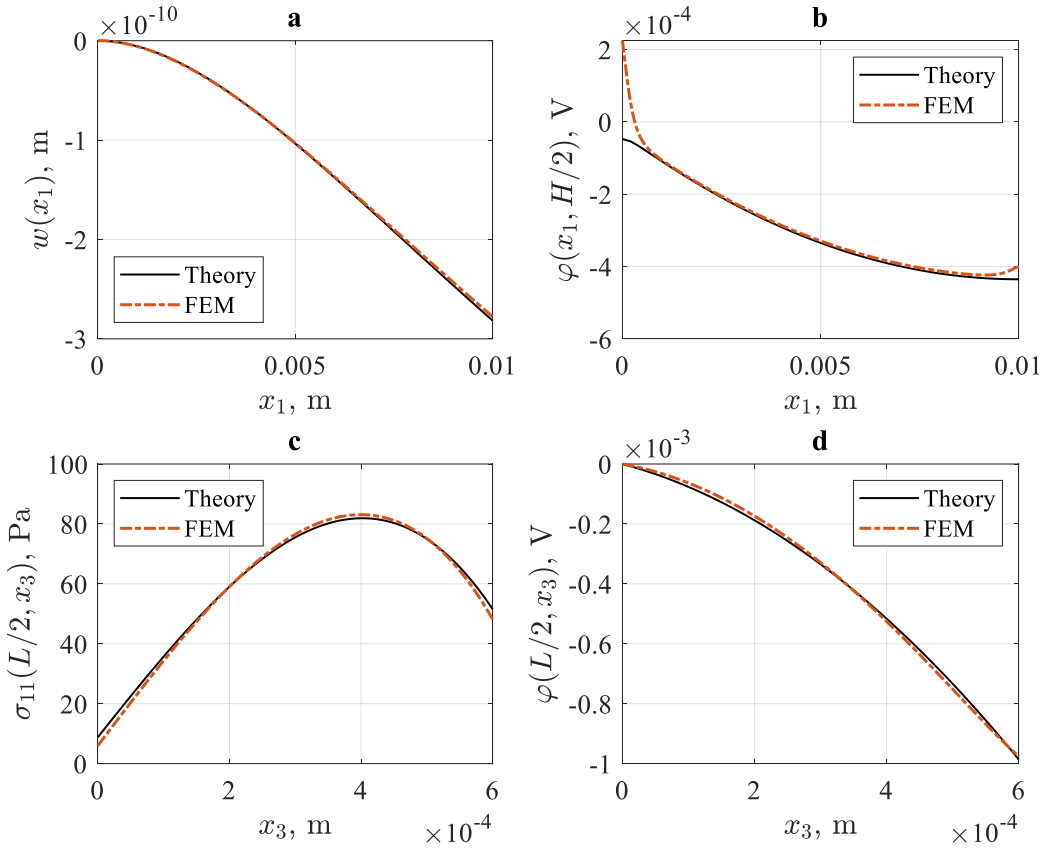

Fig. 7. Comparison of numerical results obtained on the basis of FEM and applied theory. Dependencies: a) deflection on x_1, b) electric potential on x_1 at $H/2$, c) mechanical stresses on x_3 at $L/2$, d) electric potential on x_3 at $L/2$

Table 2. Resonance frequencies

Porosity, % (out-in)	f_1, kHz FEM	f_1, kHz Theory	Error, %	f_2, kHz FEM	f_2, kHz Theory	Error, %	f_3, kHz FEM	f_3, kHz Theory	Error, %
0-50 (case I)	7.41	7.49	1.2	41.05	46.06	12.2	100.04	125.10	25
50-0 (case II)	5.78	5.72	0.9	34.25	35.37	3.2	89.13	96.92	8.7
50-50	5.40	5.46	1	31.23	33.65	7.7	79.03	91.87	16.2

As can be seen from Table 2, the applied theory determines the first resonant frequency quite well. In most applications, including energy harvesting, the first resonant frequency is the operating frequency. For a more accurate finding of the remaining frequencies, it is necessary to introduce more complex hypotheses.

At the end of the work, we study the dependence of the first resonant frequency on the degree of porosity. We will consider two cases. In the first case, the value of porosity at the plate surface varies from 0 to 80 %, and inside it is equal to zero. In the second case, the opposite is true.

An analysis of Fig. 8 allows us to conclude that in the case when the porosity near the surface is zero, but changes inside, then the first resonant frequency drops. In the second case, it starts to increase. Such trends in the future may allow, by changing the porosity, to optimize the plate for a given resonant frequency.

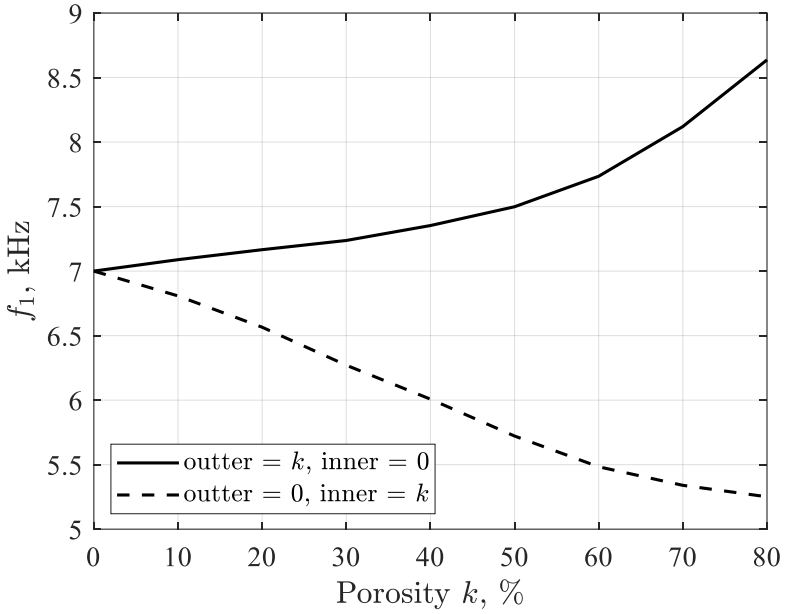

Fig. 8. Dependence of the first resonant frequency on the percentage of porosity

Conclusion

In the work, a system of ordinary differential equations with constant coefficients was obtained, which describes the bending vibrations of a FGP bimorph plate, in which the material properties are distributed according to a power quadratic law. Within the framework of this system, the nonlinear distribution of the electric potential over the thickness and length of the piezoactive layer was taken into account. Based on the developed applied theory, a study was made of the stress-strain state and the electric field of the FGP plate, as well as natural frequencies, for cases where the porosity changes from smaller near the surface of the plate to larger inside and vice versa. To verify the theory obtained, a similar problem was built in the COMSOL Multiphysics FE package.

It has been established that in the case of zero values of the electric potential on the electrodes, the latter has a pronounced non-linear character. Moreover, this nonlinearity is observed in the entire region of the plate. The use of the quadratic distribution of the electric potential in the framework of the presented theory showed good agreement between the results and the FE simulation. However, for the case when the porosity changed from greater near the surface of the plate to lesser inside, the distribution of the electric potential over the layer thickness had a complex non-linear nature, different from quadratic. In this particular case, the accepted hypotheses turned out to be insufficient. Although other characteristics were determined with acceptable accuracy. In the case of excitation of plate vibrations by induction of an electric potential, the applied theory has demonstrated good agreement between the results and the data of finite element modeling. Also, as part of the study, the problem of finding an unknown electrical potential under the influence of a mechanical load was considered, which showed good convergence with COMSOL data. In all the cases considered, the errors of the theory in the region of the embedding and the free edge of the plate were noted, which are due to the fact that the accepted hypotheses exclude shear stresses from consideration. Nevertheless, the area of these discrepancies does not exceed one plate thickness. Based on the studies carried out, it can be concluded that in the case when the gradient of material properties is significantly large, which is the subject of a separate work,

the hypothesis of a linear distribution of horizontal displacements over the thickness will probably need to be abandoned.

The study of natural frequencies based on applied theory showed that the first resonant frequency is determined with good accuracy. This is sufficient for most practical applications of such devices, since the first resonant frequency is the operating one for them. An analysis of the dependence of the first resonant frequency on porosity for two cases of its distribution showed that by changing the percentage of volumetric porosity it is possible to control the resonant frequency.

The quadratic thickness distributions of the electric potential and material constants adopted in the work showed good agreement between the results and the data of FE modeling and can be used to calculate natural oscillations and steady-state oscillations for a given difference in electrical stresses, as well as under mechanical loading.

References

1. Safaei M, Sodano HA, Anton SR. A review of energy harvesting using piezoelectric materials: state-of-the-art a decade later (2008–2018). *Smart Materials and Structures*. 2019;28(11): 113001.
2. Gaudenzi P. *Smart structures: physical behavior, mathematical modeling and applications*. New York: Wiley; 2009.
3. Shevtsov SN, Soloviev AN, Parinov IA, Cherpakov AV, Chebanenko VA. *Piezoelectric Actuators and Generators for Energy Harvesting*. Heidelberg: Springer; 2018.
4. Zhu XH, Meng Z. Operational principle, fabrication and displacement characteristics of a functionally gradient piezoelectric ceramic actuator. *Sensors Actuators A*. 1995;48: 169-76.
5. Adikary SU, Meng ZY, Jin DR. A resistivity gradient piezoelectric FGM actuator. J. Mater. Sci. Technol. 2000;16: 383-386.
6. Li JF, Takagi K, Ono M, Pan W, Watanabe R, Almajid A, Taya M. Fabrication and evaluation of porous piezoelectric ceramics and porosity-graded piezoelectric actuators. *J. Am. Ceram. Soc*. 2003;86: 1094-1098.
7. Qiu J, Tani J, Ueno T, Morita T, Takahashi H, Du HJ. Fabrication and high durability of functionally graded piezoelectric bending actuators. *Smart Mater. Struct*. 2003;12: 115-121.
8. Li JF, Zhang HL, Takagi K, Watanabe R. Design, processing and evaluation of graded piezoelectric ceramic bending actuators. *Key Eng. Mater*. 2005; 280-283: 1857-1862.
9. Heyliger PR, Brooks SB. Exact free vibration of piezoelectric laminates in cylindrical bending. *International Journal of Solids and Structures*. 1995;32(20): 2945-2960.
10. Ray MC, Rao KM, Samanta B. Exact solution for static analysis of an intelligent structure under cylindrical bending. *Computers & Structures*. 1993;47(6): 1031-1042.
11. Saravanos DA, Heyliger PR. Mechanics and computational models for laminated piezoelectric beams, plates, and shells. *Applied Mechanics Reviews*. 1999;52(10): 305-320.
12. Sung CK, Chen TF, Chen SG. Piezoelectric modal sensor/actuator design for monitoring/generating flexural and torsional vibrations of cylindrical shells. *Journal of Vibration and Acoustics.* 1996;118(1): 48-55.
13. Kogl M, Bucalem ML. Analysis of smart laminates using piezoelectric MITC plate and shell elements. *Computers & Structures*. 2005;83(15-16): 1153-1163.
14. Allik H, Hughes TJR. Finite element method for piezoelectric vibration. *International Journal for Numerical Methods in Engineering*. 1970;2(2): 151-157.
15. Benjeddou A. Advances in piezoelectric finite element modeling of adaptive structural elements: a survey. *Computers & Structures*. 2000;76(1-3): 347-363.
16. Sheikh AH, Topdar P, Halder S. An appropriate FE model for through thickness variation of displacement and potential in thin/moderately thick smart laminates. *Composite Structures*. 2001;51(4): 401-409.

17. Benjeddou A, Trindade MA, Ohayon RA. A unified beam finite element model for extension and shear piezoelectric actuation mechanisms. *Journal of Intelligent Material Systems and Structures*. 1997;8(12): 1012-1025.
18. Soloviev AN, Chebanenko VA, Parinov IA. Mathematical Modelling of Piezoelectric Generators on the Base of the Kantorovich Method. In: Altenbach H, Carrera E, Kulikov G (Eds.) *Analysis and Modelling of Advanced Structures and Smart Systems*. Singapore: Springer; 2018. p.227-258.
19. Maurini C, Pouget J, dell'Isola F. Extension of the Euler–Bernoulli model of piezoelectric laminates to include 3D effects via a mixed approach. *Computers & Structures*. 2006;84(22-23): 1438-1458.
20. Kapuria S, Kumari P, Nath JK. Efficient modeling of smart piezoelectric composite laminates: a review. *Acta Mechanica*. 2010;214(1-2): 31-48.
21. Vatul'yan AO, Getman IP, Lapitskaya NB. Flexure of a piezoelectric bimorphic plate. *Soviet Applied Mechanics*. 1991;27(10): 1016-1019.
22. Vatul'yan AO, Rynkova AA. Flexural vibrations of a piezoelectric bimorph with a cut internal electrode. *Journal of Applied Mechanics and Technical Physics*. 2001;42(1): 164-168.
23. Shi ZF, Chen Y. Functionally graded piezoelectric cantilever beam under load. *Archive of Applied Mechanics.* 2004;74: 237-247.
24. Yang J, Xiang HJ. Thermo-electro-mechanical characteristics of functionally graded piezoelectric actuators. *Smart Mater. Struct*. 2007;16: 784-797.
25. Liu Y, Qin Z, Chu F. Nonlinear forced vibrations of functionally graded piezoelectric cylindrical shells under electric-thermo-mechanical loads. *International Journal of Mechanical Sciences.* 2021;201: 106474.
26. Wang Q, Zhong R, Qin B, Yu H. Dynamic analysis of stepped functionally graded piezoelectric plate with general boundary conditions. *Smart Materials and Structures.* 2020;29(3): 03502227.
27. Zenkour AM, Hafed ZS. Bending analysis of functionally graded piezoelectric plates via quasi-3D trigonometric theory. *Mechanics of Advanced Materials and Structures.* 2020;27(18): 1551-1562.
28. Shen Y, Zhang P, He W, Xu M, Duan Q. Transverse vibration responses of the in-plane-wise functionally graded piezoelectric composite plates. *Mechanics of Advanced Materials and Structures*. 2023;30(3): 592-608.
29. Wang YQ. Electro-mechanical vibration analysis of functionally graded piezoelectric porous plates in the translation state. *Acta Astronautica*. 2018;143: 263-271.
30. Nguyen LB, Thai CH, Zenkour AM, Nguyen-Xuan H. An isogeometric Bézier finite element method for vibration analysis of functionally graded piezoelectric material porous plates. *International Journal of Mechanical Sciences*. 2019;157: 165-183.
31. Kumar P, Harsha A. Vibration response analysis of the bi-directional porous functionally graded piezoelectric (BD-FGP) plate. To be published in *Mechanics Based Design of Structures and Machines*. 2022.
32. Heshmati M, Amini YJ. A comprehensive study on the functionally graded piezoelectric energy harvesting from vibrations of a graded beam under travelling multi-oscillators. *Applied Mathematical Modelling*. 2019;66: 344-361.
33. Yu P, Leng W, Peng L, Suo Y, Guo J. The bending and vibration responses of functionally graded piezoelectric nanobeams with dynamic flexoelectric effect. Results in Physics. 2021;28: 104624.
34. Wang Z, Maruyama K, Narita F. A novel manufacturing method and structural design of functionally graded piezoelectric composites for energy-harvesting. *Materials & Design*. 2022; 214: 110371.

35. Soloviev AN, Chebanenko VA, Parinov IA, Oganesyan PA. Applied theory of bending vibrations of a piezoelectric bimorph with a quadratic electric potential distribution. *Materials Physics and Mechanics.* 2019;42(1): 65-73.
36. Nasedkin AV, Oganesyan PA, Soloviev AN. Analysis of Rosen type energy harvesting devices from porous piezoceramics with great longitudinal piezomodulus. *ZAMM-Journal of Applied Mathematics and Mechanics/Zeitschrift für Angewandte Mathematik und Mechanik.* 2021;101(3): e202000129.
37. Nowacki W. Mathematical models of phenomenological piezoelectricity. *Banach Center Publications.* 1985;1(15): 593-607.
38. Soloviev AN, Do BT, Chebanenko VA, Parinov IA. Flexural Vibrations of a Composite Piezoactive Bimorph in an Alternating Magnetic Field: Applied Theory and Finite-Element Simulation. *Mechanics of Composite Materials.* 2022;58(4): 471-482.

THE AUTHORS

Soloviev A.N.
e-mail: solovievarc@gmail.com

Chebanenko V.A.
e-mail: valera.chebanenko@yandex.ru